Optica Applicata, Vol. XXXV, No. 2, 2005

Theoretical study on wavelength conversion using cross-polarization modulation in a single semiconductor optical amplifier

FEI WANG, GUANGQIONG XIA, ZHENGMAO WU

School of Physics, Southwest Normal University, Chongqing 400715, P.R. China;
e-mail: zmwu@swnu.edu.cn

Wavelength conversion based on the cross-polarization modulation (XPM) in a single semiconductor optical amplifier (SOA) has been numerically investigated by using the theoretical model in which the birefringence has been taken into account. The results show that the non-inverted and inverted wavelength conversion can be realized through selecting reasonably the parameters; there exit some differences in the chirp, extinction ratio (ER), and eye diagram of the converted signal between the non-inverted and inverted conversion; with the increase of the bit rate, the chirp increases and the eye opening ratio (EOR) decreases.

Keywords: wavelength conversion, cross-polarization modulation, semiconductor optical amplifier.

1. Introduction

In the wavelength division multiplexing (WDM) system, it is necessary to use wavelength converters for frequency reuse and wavelength/spatial routing. To implement all optical wavelength converters, several promising techniques relying on cross-gain modulation (XGM) [1, 2], cross-phase modulation [3, 4], and four-wave mixing [5, 6] in a single semiconductor optical amplifier (SOA) have been reported. Among these methods, the XGM method is the simplest to realize and has shown impressive performance for bit rate up to 40 Gb/s. However, it has two obvious shortcomings: the converted signal has a relatively large chirp and the extinction ratio (ER) can significantly be degraded when the signal is wavelength up-converted. To overcome these problems, the cross-polarization modulation (XPM) method has been presented and investigated [7–9]. However, the related theoretical works are inadequate. In this paper, the chirp, the extinction ratio (ER) and eye diagram for non-inverted and inverted wavelength conversion based on the XPM method in a single SOA have been investigated numerically by using the theoretical model in which the birefringence was taken into account [10].

2. Theory

The schematic of all-optical wavelength converter (AOWC) is shown in Fig. 1. A laser emits a continuous wave CW probe beam at wavelength λ_{probe} that is fed into a SOA (with a strained bulk active region), the output from the SOA is sent into a polarization beam splitter PBS. The first polariztion controller PC1 is used to adjust polarization of the input signal to be approximately 45° to the orientation of the SOA layers, while the second polariztion controller PC2 is used to adjust the polarization of the amplified SOA output to the orientation of the PBS. The SOA can be saturated by injecting a high-intensity pump signal at a different wavelength λ_{pump}. The injection pump light introduces additional birefringence in the SOA [11], which causes the TE and TM modes of the probe beam to experience a different refractive index. At the PBS, the two modes coherently combine.

As shown in Fig. 2, the incoming arbitrarily polarized electric field is decomposed into a component parallel to the layers in the waveguide (TE mode) and a perpendicular

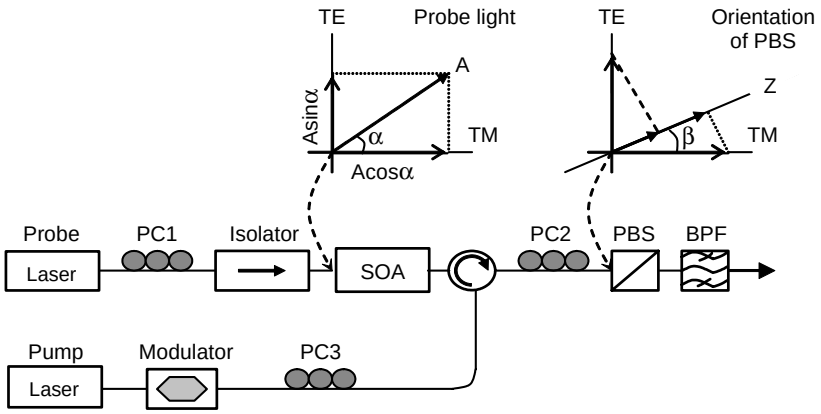

Fig. 1. Schematic of the all-optical wavelength converter; PC – polarization controllers, BPF – optical bandpass filter, PBS – polarization beam splitter, SOA – semiconductor optical amplifier.

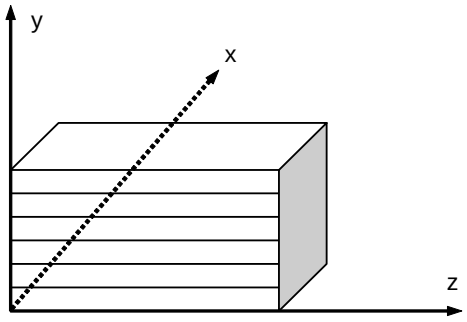

Fig. 2. Waveguide structure and definition of coordinate frame.

component (TM mode). These two polarization directions are along the principal axes that diagonalize the wave propagation in the SOA.

In this paper, to simplify the discussions, the spontaneous emission in the SOA has been ignored. The propagation equation for the transverse electric (TE) component $A^{\mathrm{TE}}(z, t)$ and the transverse magnetic (TM) component $A^{\mathrm{TM}}(z, t)$ is given by

$$\left(\frac{\partial}{\partial t} + v_g^{\mathrm{TE}}\frac{\partial}{\partial z}\right)A^{\mathrm{TE}}(z, t) = \frac{1}{2}\Gamma^{\mathrm{TE}}(1 + i\alpha^{\mathrm{TE}})\, g^{\mathrm{TE}}(z, t)\, A^{\mathrm{TE}}(z, t) - \frac{1}{2}\alpha_{\mathrm{int}}^{\mathrm{TE}} A^{\mathrm{TE}}(z, t), \tag{1}$$

$$\left(\frac{\partial}{\partial t} + v_g^{\mathrm{TM}}\frac{\partial}{\partial z}\right)A^{\mathrm{TM}}(z, t) = \frac{1}{2}\Gamma^{\mathrm{TM}}(1 + i\alpha^{\mathrm{TM}})\, g^{\mathrm{TM}}(z, t)\, A^{\mathrm{TM}}(z, t) - \frac{1}{2}\alpha_{\mathrm{int}}^{\mathrm{TM}} A^{\mathrm{TM}}(z, t) \tag{2}$$

where the superscript TE and TM characterize the transverse electric and the transverse magnetic component, respectively, $A(z, t)$ is the weakly time and space-dependent complex envelope of the optical field, v_g is the corresponding group velocity taken at the central frequency of the wave, Γ is the confinement factor, $g(z, t)$ is the gain function, α is the phase-modulation parameter, and α_{int} is the modal loss, and the envelopes for each polarization can be expressed as

$$\begin{aligned} A^{\mathrm{TE}}(z, t) &= \sqrt{S^{\mathrm{TE}}(z, t)}\, \exp\left[i\phi^{\mathrm{TE}}(z, t)\right], \\ A^{\mathrm{TM}}(z, t) &= \sqrt{S^{\mathrm{TM}}(z, t)}\, \exp\left[i\phi^{\mathrm{TM}}(z, t)\right] \end{aligned} \tag{3}$$

where $S(z, t)$ is the intensity and $\phi(z, t)$ is the phase, and the gain $g(z, t)$ for the TE and TM polarization are given by

$$g^{\mathrm{TE}}(z, t) = \xi^{\mathrm{TE}}\left[n_c(z, t) + n_x(z, t) - N_0\right], \tag{4}$$

$$g^{\mathrm{TM}}(z, t) = \xi^{\mathrm{TM}}\left[n_c(z, t) + n_y(z, t) - N_0\right] \tag{5}$$

where ξ is the gain coefficient, $n_c(z, t)$ is the number of electrons in the conduction band, $n_x(z, t)$ and $n_y(z, t)$ are the number of holes involved in the x and y transitions, respectively, N_0 is the total number of electronic states involved in the optical transition. In cases of high-intensity optical beams, one should correct ξ^{TE}, ξ^{TM} for saturation due to the carrier heating according to

$$\xi^{\mathrm{TE}} = \frac{\xi_0^{\mathrm{TE}}}{1 + \varepsilon S^{\mathrm{TE}}}, \qquad \xi^{\mathrm{TM}} = \frac{\xi_0^{\mathrm{TM}}}{1 + \varepsilon S^{\mathrm{TM}}} \tag{6}$$

where ξ_0 is differential gain coefficient in a small-signal, ε is typically 10^{-7} per photon in the SOA [12]. If we assume that the total number of holes is equal to the number of electrons

$$n_c(z, t) = n_x(z, t) + n_y(z, t). \tag{7}$$

Substituting (7) into (4) and (5), $g^{\mathrm{TE}}(z, t)$ and $g^{\mathrm{TM}}(z, t)$ can be expressed as

$$g^{\mathrm{TE}}(z, t) = \xi^{\mathrm{TE}}\Big[2n_x(z, t) + n_y(z, t) - N_0\Big], \tag{8}$$

$$g^{\mathrm{TM}}(z, t) = \xi^{\mathrm{TM}}\Big[2n_y(z, t) + n_x(z, t) - N_0\Big]. \tag{9}$$

Then, the rate-equation for $n_x(z, t)$, $n_y(z, t)$ can be written as [10]

$$\frac{\partial n_x(z, t)}{\partial t} = -\frac{n_x(z, t) - \overline{n_x}}{T_1} - \frac{n_x(z, t) - f n_y(z, t)}{T_2} - g^{\mathrm{TE}}(z, t) S^{\mathrm{TE}}(z, t), \tag{10}$$

$$\frac{\partial n_y(z, t)}{\partial t} = -\frac{n_y(z, t) - \overline{n_y}}{T_1} - \frac{f n_y(z, t) - n_x(z, t)}{T_2} - g^{\mathrm{TM}}(z, t) S^{\mathrm{TM}}(z, t) \tag{11}$$

where $\overline{n_x}$ and $\overline{n_y}$ are the respective equilibrium values determined by the applied pump current as will be discussed below, the last term in the right-hand side of Eqs. (10) and (11) accounts for the stimulated recombination, T_1 is the electron-hole recombination time (usually, T_1 is relevant to the construction of the semiconductor and the carrier density; for simplicity, T_1 is assumed to be independent of the carrier density in this paper), T_2 is the inter-hole relaxation time with typically timescale 50–100 fs, f is the hole population imbalance factor. It should be noted that the inter-hole relaxation time T_2 is much shorter than the electron recombination time T_1 (about hundreds of ps) and the two populations n_x and n_y will be clamped tightly together, *i.e.*,

$$n_x(z, t) = f n_y(z, t) \tag{12}$$

where f expresses the magnitude of the anisotropy. For the unstrained bulk material, the gain will be isotropic, *i.e.*, $f = 1$, while for the tensile strain, TM gain will be larger than TE, *i.e.*, $f < 1$. For the equilibrium values, consistent with (12), we can write

$$\overline{n_x} = \frac{\overline{n} f}{1 + f}, \qquad \overline{n_y} = \frac{\overline{n}}{1 + f} \tag{13}$$

where

$$\overline{n} = \frac{I}{e} T_1 \tag{14}$$

while I is the electric current and e is the electric unit charge.

The optical power $P^{\mathrm{TE/TM}}$ for each mode is related to the intensity $S^{\mathrm{TE/TM}}$ according to

$$S^{\mathrm{TE/TM}} = \frac{P^{\mathrm{TE/TM}}}{\hbar\omega}\frac{L}{v_g^{\mathrm{TE/TM}}} \tag{15}$$

where $\hbar$ is Planck's constant, ω is the optical frequency, and L is the length of the SOA. The propagation equation of phase for the TE and TM modes can be expressed as

$$\begin{aligned}\frac{\partial\phi^{\mathrm{TE}}(z,t)}{\partial z} &= \frac{1}{2}\frac{\alpha^{\mathrm{TE}}\Gamma^{\mathrm{TE}}g^{\mathrm{TE}}(z,t)}{v_g^{\mathrm{TE}}},\\ \frac{\partial\phi^{\mathrm{TM}}(z,t)}{\partial z} &= \frac{1}{2}\frac{\alpha^{\mathrm{TM}}\Gamma^{\mathrm{TM}}g^{\mathrm{TM}}(z,t)}{v_g^{\mathrm{TM}}}.\end{aligned} \tag{16}$$

So, the complex envelope of the probe optical field out from the PBS can be written as

$$A_{\mathrm{out}} = \sqrt{S_{\mathrm{out}}^{\mathrm{TE}}}\sin\beta\exp\left[i\left(\phi^{\mathrm{TE}}+\phi_{\mathrm{PC}}\right)\right] + \sqrt{S_{\mathrm{out}}^{\mathrm{TM}}}\cos\beta\exp\left(i\phi^{\mathrm{TM}}\right) \tag{17}$$

with

$$\begin{aligned}S_{\mathrm{out}}^{\mathrm{TE}} &= S_{\mathrm{in}}\cos^2\alpha\exp\left[\frac{\left(\Gamma^{\mathrm{TE}}g^{\mathrm{TE}}-\alpha_{\mathrm{int}}^{\mathrm{TE}}\right)L}{v_g^{\mathrm{TE}}}\right],\\ S_{\mathrm{out}}^{\mathrm{TM}} &= S_{\mathrm{in}}\sin^2\alpha\exp\left[\frac{\left(\Gamma^{\mathrm{TM}}g^{\mathrm{TM}}-\alpha_{\mathrm{int}}^{\mathrm{TM}}\right)L}{v_g^{\mathrm{TM}}}\right]\end{aligned} \tag{18}$$

where S_{in} represents the intensity of the probe beam at the SOA input, β is the angle between the orientation of the PBS and the SOA layers, ϕ is the phase of the probe beam obtained from the SOA, ϕ_{PC} is the linear phase induced by PC1 and PC2. The chirp of the output signal can be expressed as

$$\Delta\nu = -\frac{1}{2\pi}\frac{\mathrm{d}\phi}{\mathrm{d}t} \tag{19}$$

here ϕ is the phase of the probe optical field output from the PBS.

T a b l e. SOA parameter definitions and their values.

Parameter	Symbol	Value	Units
Confinement factor	Γ^{TE}, Γ^{TM}	0.2, 0.14	
Phase modulation coefficients	a^{TE}, a^{TM}	7, 7	
Modal loss	α_{int}^{TE}, α_{int}^{TM}	0.175, 0.175	ps^{-1}
Small-signal gain coefficient	ξ_0^{TE}, ξ_0^{TM}	5.5, 5.5	10^{-9} ps^{-1}
Hole population imbalance factor	f	0.8	
Electron-hole recombination time	T_1	350	ps
Hole-hole relaxation time	T_2	0.1	ps
Optical transition state number	N_0	1.875×10^8	
Group velocity	v_g^{TE}, v_g^{TM}	100	μm/ps
SOA length	L	800	μm

Based on the above analysis, the wavelength conversion based on the cross-polarization modulation (XPM) in a single SOA can be numerically investigated. The SOA parameters and their physical definitions are listed in the Table [13].

3. Results and discussion

The probe polarization direction is adjusted to 45° with the SOA layers by using the PC1, and the polarization orientation of the signal is adjusted to be parallel to the SOA layers by using the PC3 [14]. The function of the PC2 is twofold: firstly, it determines

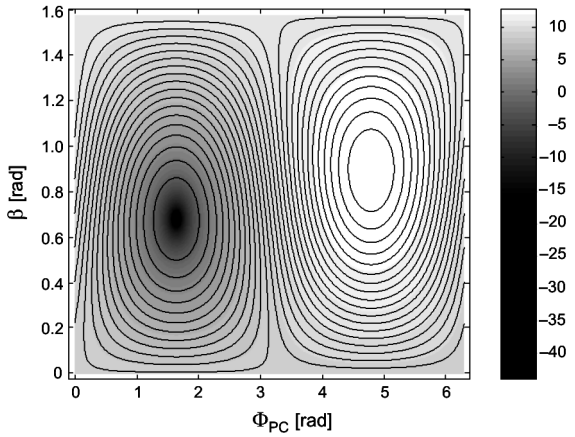

Fig. 3. Contour plot of the probe power out from the PBS with β and Φ_{PC} (I = 399 mA, λ_{pump} = 1550.92 nm, λ_{probe} = 1552.60 nm, P_{CW} = 3.82 dBm).

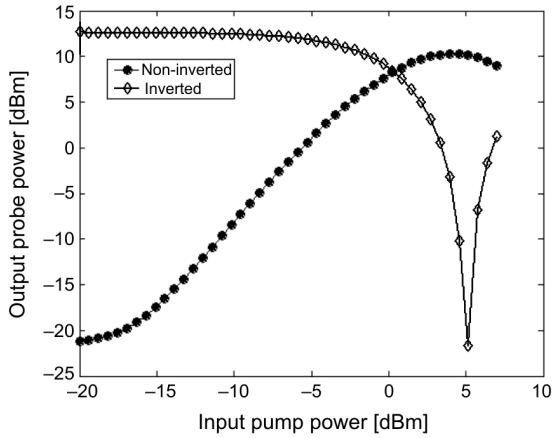

Fig. 4. Simulated output power of the probe light *vs.* the input power of the pump light (I = 399 mA, λ_{pump} =1550.92 nm, λ_{probe} =1552.60 nm, P_{CW} = 3.82 dBm).

β in the Eq. (17) because PC2 can change the polarization of the SOA output into any desired polarization. In addition, it induces an extra phase Φ_{PC} by changing the stress to the fiber in PC2. At this point, PC2 acts as a phase compensator.

Figure 3 shows contour plot of the probe power out of the PBS with β and Φ_{PC}. To realize non-inverted (or inverted) wavelength conversion, firstly, without the pump light, the probe power output from the PBS must be adjusted to the minimum (or the maximum) by changing the β and Φ_{PC}. If a saturating pump beam is coupled into the SOA, the additional birefringence in the SOA leads to a phase difference between TE and TM modes of the probe light, causing the polarization of the probe light to be rotated [7, 8]. As a consequence, the magnitude of the probe light passed through the PBS will increase (non-inverted) or decrease (inverted), thus the non-inverted or inverted wavelength conversion are obtained. Calculation shows that the probe power output from the PBS may reach its maximum when Φ_{PC} = 4.80 rad and β = 0.90 rad; and when Φ_{PC} = 1.65 rad, β = 0.70 rad, the probe power output from the PBS may reach its minimum.

Figure 4 shows the power of the probe light output from PBS *vs.* the power of the pump light for the inverted and non-inverted wavelength conversion. The power of the probe light that enters the SOA is 3.82 dBm, and the SOA is pumped with 399 mA of current. The results of our simulation are similar to the experimental results in the Fig. 2 of the reference [15], in which the power of the probe light is 2 dBm, and the SOA is pumped with 237 mA of current. It can be seen from Fig. 4 that the extinction ratio (ER) of the converted signal can be over 20 dB. In the wavelength converter, in order to saturate the SOA, the intensity of the pump light must be high enough, so XGM takes place simultaneously with nonlinear polarization rotation. XGM opposes the effect of non-inverted wavelength conversion, but enlarges the effect of inverted wavelength conversion. As a consequence, the slope of the curve for the inverted case is sharper than that of the non-inverted case [15].

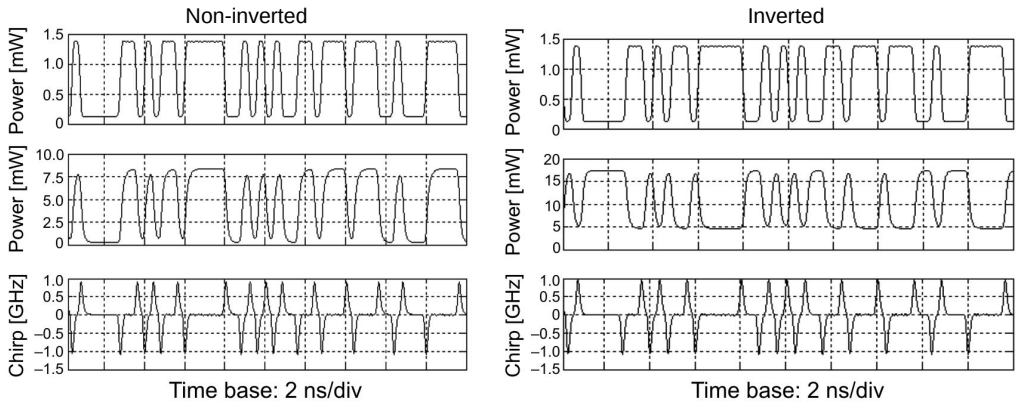

Fig. 5. Input signal pulse pattern (up), the converted signal pulse pattern (middle), and the frequency chirp (low) of the XPM wavelength converter (P_{SIG} = –1.22 dBm and ER_{SIG} = 10 dB).

Figure 5 shows the simulated input pulse pattern, output pulse pattern and chirp frequency of the converted signal for the non-inverted and inverted operation. Pseudorandom bit sequence (PRBS) signal bit rate of the $2^7 - 1$ word length is used as the input signal (P_{SIG} = –1.22 dBm, ER_{SIG} = 10 dB). From this diagram, it can be seen that the converted signal undergoes a red shift (about 0.92 GHz) during the rising edge and a blue shift (about –1.10 GHz) during the falling edge for non-inverted operation. While, the converted signal has a blue shift (about 0.98 GHz) during the rising edge and a red shift (about –1.11 GHz) during the falling edge for the inverted operation.

The eye diagrams for the non-inverted and inverted conversion are presented in the Figs. 6**a** and 6**b**, respectively. Calculation shows that the eye opening ratio (EOR) of the output signals on the non-inverted operation is 10.45 dB (P_{SIG} = –1.22 dBm, ER_{SIG} = 10 dB), and EOR of the output signals on the inverted operation is 5.28 dB. The eye diagram for inverted conversion has a fast fall time but slow rise time, which

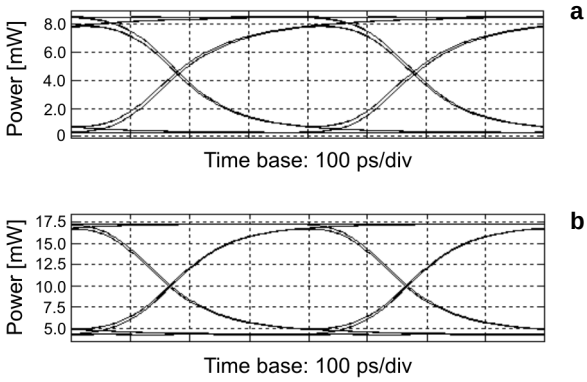

Fig. 6. Eye diagrams for wavelength conversion at 2.5Gbit/s: non-inverted (**a**) and inverted signal (**b**).

can be explained by the nonlinear slope in the transfer curve (see Fig. 4) in combination with the slow carrier recovery time of the SOA.

Figure 7 shows peak chirp and extinction ratio of the converted signals as a function of the input signal power. The input signal bit rate is assumed to be 2.5 Gbit/s, and the extinction ratio (ER) of the input signal is 10 dB. Figure 7**a** is for the non-inverted case, there is a signal power corresponding to the peak ER of the output signal (> 14 dB), and is defined as $P_{S,\,\mathrm{peak}}$, nearby which the frequency chirp is lower. Figure 7**b** is for the inverted case, with the increase in the input signal power, the ER drastically increases at first, after passing a peak value, and decreases quickly, while the peak chirp increases. The ER of the output signal change with the input pump power can be interpreted by the curves in the Fig. 4. The increase in the carrier-photon interaction due to the increase in input pump power results in the increase of the chirp.

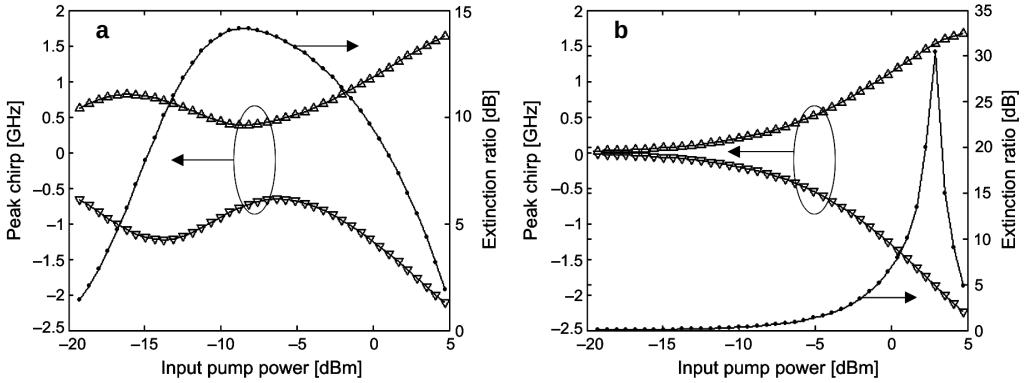

Fig. 7. Peak chirp and the extinction ratio of the converted signals as a function of input pump power (I = 399 mA, P_{CW} = 3.82 dBm, $\mathrm{ER_{SIG}}$ = 10 dB): non-inverted (**a**) and inverted (**b**).

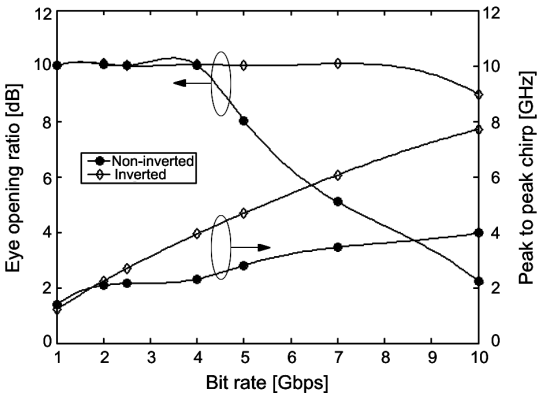

Fig. 8. Eye opening ratio and peak-to-peak chirp under the inverted operation as a function of the data rate (I = 399 mA, P_{CW} = 3.82 dBm, $\mathrm{ER_{SIG}}$ = 10 dB).

Figure 8 shows the eye opening ratio and peak-to-peak chirp as a function of the data rate (I = 399 mA, P_{CW} = 3.82 dBm, ER_{SIG} = 10 dB). It should be pointed out that during simulating this diagram, the ERs of output signals are always maintained to 10 dB by adjusting input pump power. From this diagram, it can be seen that the peak-to-peak chirps and EORs of the output pulse for non-inverted and inverted conversion are nearly equal when the bit rate of signal is small; while the bit rate increases, the deficit between the inverted and non-inverted conversion will also increase. The chirp and the EOR of pulse for inverted conversion are more than that of the pulse for non-inverted conversion. The EOR starts to decrease quickly when the bit rate is more than 7 Gbit/s for inverted or 4 Gbit/s for non-inverted conversion, respectively.

4. Conclusions

In this paper, the performances of wavelength conversion based on the XPM in a single SOA have been investigated numerically. Through selecting reasonably the value of β and Φ_{PC}, the non-inverted and inverted wavelength conversion can be realized. The chirp, the extinction ratio and eye diagram of the output for non-inverted conversion are different from that of the output for the inverted case. When the bit rate increases from 1 to 10 Gbit/s, the chirp also increases and the EOR decreases for both non-inverted and inverted wavelength conversion.

Acknowledgement – The authors gratefully acknowledge the support from the Commission of Science and Technology of Chongqing City of P. R. China, the Key Project of Chinese Ministry of Education (Grant No. 03140) and the Ph.D. Fund of the Southwest Normal University, P.R. China.

References

[1] ASGHARI M., WHITE I.H., PENTY R.V., *Wavelength conversion using semiconductor optical amplifiers*, Journal of Lightwave Technology **15**(7), 1997, pp. 1181–90.

[2] YOO S.J.B., *Wavelength conversion technologies for WDM network applications*, Journal of Lightwave Technology **14**(6), 1996, pp. 955–66.

[3] DURHUUS T, MIKKELSEN B., JOERGENSEN C., DANIELSEN S.L., STUBKJAER K.E., *All-optical wavelength conversion by semiconductor optical amplifiers*, Journal of Lightwave Technology **14**(6), 1996, pp. 942–54.

[4] YE Y., ZHENG X., ZHANG H., LI Y., GUO Y., *Theoretical study on wavelength conversion based on cross phase modulation using semiconductor optical amplifiers*, International Journal of Infrared and Millimeter Waves **22**(12), 2001, pp. 1785–93.

[5] ZHOU J., PARK N., VAHALA K.J., NEWKIRK M.A., MILLER B.I., *Four-wave mixing wavelength conversion efficiency in semiconductor traveling-wave amplifiers measured to 65 nm of wavelength shift*, IEEE Photonics Technology Letters **6**(8), 1994, pp. 984–7.

[6] LACEY J.P.R., SUMMERFIELD M.A., MADDEN S.J., *Tunability of polarization-insensitive wavelength converters based on four-wave mixing in semiconductor optical amplifiers*, Journal of Lightwave Technology **16**(12), 1998, pp. 2419–27.

[7] STEPHENS M.F.C., ASGHARI M., PENTY R.V., WHITE I.H., *Demonstration of ultrafast all-optical wavelength conversion utilizing birefringence in semiconductor optical amplifiers*, IEEE Photonics Technology Letters **9**(4), 1997, pp. 449–51.
[8] SOTO H., ERASME D., GUEKOS G., *Cross-polarization modulation in semiconductor optical amplifiers*, IEEE Photonics Technology Letters **11**(8), 1999, pp. 970–2.
[9] LEE H.J., SOHN M., KIM K., KIM H.G., *Wavelength dependent performance of a wavelength converter based on cross-gain modulation and birefringence of a semiconductor optical amplifier*, IEEE Photonics Technology Letters **11**(2), 1999, pp. 185–7.
[10] LENSTRA D., LIU Y., HILL M.T., KHOE G.D., DORREN H.J.S., *Nonlinear polarization rotation in semiconductor optical amplifiers: Theory and application to all-optical flip-flop memories*, IEEE Journal of Quantum Electronics **39**(1), 2003, pp. 141–8.
[11] MANNING R.J., ANTONOPOULOS A., LE ROUX R., KELLY A.E., *Experimental measurement of nonlinear polarisation rotation in semiconductor optical amplifiers*, Electronics Letters **37**(4), 2001, pp. 229–31.
[12] AGRAWAL G.P., DUTTA N.K., *Long-wavelength semiconductor lasers*, Van Nostrand, New York 1986.
[13] YANG X., LENSTRA D., KHOE G.D., DORREN H.J.S., *Nonlinear polarization rotation induced by ultrashort optical pulses in a semiconductor optical amplifier*, Optics Communications **223**(1-3), 2003, pp. 169–79.
[14] MISHRA A.K., YANG X., LENSTRA D., KHOE G.D., DORREN H.J.S., *Ultrafast all-optical wavelength conversion using 160 fs pulses in a multi-quantum-well SOA*, Proc. Symposium IEEE/LEOS Benelux Chapter, Enschede, The Netherlands, 2003, pp. 205–8.
[15] LIU Y., HILL M.T., TANGDIONGGA E., DE WAARDT H., CALABRETTA N., KHOE G.D., DORREN H.J.S., *Wavelength conversion using nonlinear polarization rotation in a single semiconductor optical amplifier*, IEEE Photonics Technology Letters **15**(1), 2003, pp. 90–2.

Received September 10, 2004
in revised form February 4, 2005